ACS APPLIED MATERIALS & INTERFACES

Research Article

www.acsami.org

Evolution of Li_2O_2 Growth and Its Effect on Kinetics of Li–O_2 Batteries

Chun Xia,*[,†] Michael Waletzko,[†] Limei Chen,[‡] Klaus Peppler,[†] Peter. J. Klar,[‡] and Jürgen Janek*[,†]

[†]Institute of Physical Chemistry, Justus-Liebig-University Giessen, Heinrich-Buff-Ring 58, 35392 Giessen, Germany

[‡]Institute of Experimental Physics I, Justus-Liebig-University Giessen, Heinrich-Buff-Ring 16, 35392 Giessen, Germany

Supporting Information

ABSTRACT: Lithium peroxide (Li_2O_2), the solid and intrinsically electronic insulating discharge product of Li–O_2 batteries strongly influences the discharge and charge kinetics. In a series of experiments, we investigated the growth of Li_2O_2 upon discharge and the corresponding reduction and oxidation processes by varying the depth of discharge. The results indicate that insulating Li_2O_2 particles with a disc-like shape were formed during the initial discharge stage. Afterward, the nucleation and growth of Li_2O_2 resulted in the formation of conducting Li_2O_2 shells. When the discharge voltage dropped below 2.65 V, the Li_2O_2 discs evolved to toroid-shaped particles and defective superoxide-like phase presumably with high conductivity was formed on the rims of Li_2O_2 toroids. Both Li_2O_2 and the superoxide-like phase are unstable in ether-based electrolytes resulting in the degradation of the corresponding cells. Nevertheless, by controlling the growth of Li_2O_2, the chemical reactivity of the discharge product can be suppressed to improve the reversibility of Li–O_2 batteries.

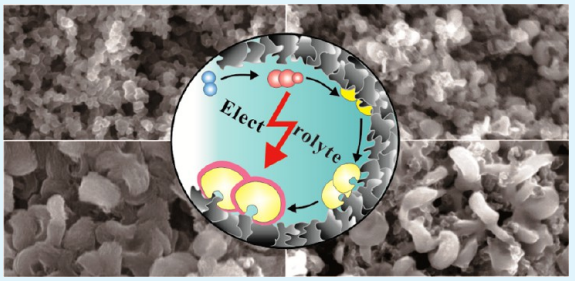

KEYWORDS: *electrochemical growth, oxidation, Li_2O_2 toroid, lithium superoxide, electrolyte decomposition, metal-air battery*

INTRODUCTION

Since the first nonaqueous lithium–oxygen cell was demonstrated by Abraham and Jiang in 1996, this type of cell has attracted worldwide interest as it theoretically should yield an energy density of about 1 order of magnitude higher than commercial lithium ion batteries.[1,2] Although the research efforts increased considerably during the past few years, it has also become obvious that the development of a truly rechargeable Li-oxygen cell is by far less straightforward than initially thought. Major fundamental and technological problems are still not solved, e.g., the poor cycling performance.[3]

As widely reported in the literature,[4] nonaqueous Li–O_2 batteries show very high overpotentials at their cathodes (typically about 0.3 V on discharge and more than 1 V on charge) which—together with the formation of chemically highly reactive intermediates—causes the instability of battery components, in particular, of the electrolyte.[5] To lower the overpotentials, extensive efforts have been made identifying effective electrocatalysts to improve the kinetics of the oxygen reduction reaction (ORR) and the oxygen evolution reaction (OER).[6−8] However, most of the electrocatalysts do not reduce the overpotentials sufficiently and often even catalyze the decomposition of electrolyte rather than the expected ORR/OER.[9]

In a previous paper,[10] we demonstrated that catalytically inert silica nanoparticles surprisingly decrease the overpotential and increase the capacity of oxygen cathodes, thereby acting as structure promoter for the growth of Li_2O_2 which leads to a "catalysis-like" effect. The function of these silica "nanocatalysts" is still not completely understood and surely needs further investigations. However, it is well accepted today that the high overpotentials of Li–O_2 batteries are mainly due to the electron transport barrier of the poorly conducting Li_2O_2 discharge product and the side products from Li_2O_2 (or LiO_2) induced carbon and electrolyte decomposition rather than to the slow surface kinetics.[11,12] This conclusion is also supported by the experimental observation that the overpotentials are significantly lowered by accelerating the charge transfer using a charge agent.[13] It is evident that the properties of the Li_2O_2 product, e.g., its electronic conductivity and chemical reactivity, directly influence the performance of Li–O_2 batteries. Therefore, a better understanding of how to control these properties of Li_2O_2 is the key to improve the reversibility of the ORR/OER in lithium–oxygen batteries. In the present work, we investigated the evolution of Li_2O_2 growth during discharge and of the corresponding oxidation process upon charging. The variations of the structural, morphological, and electrochemical properties of Li_2O_2 during discharge were examined. Based on the experimental observations, we propose some measures to improve the stability of Li–O_2 batteries.

EXPERIMENTAL SECTION

Carbon Cathode Preparation. 85 mg commercial Ketjenblack 600JD carbon (KB carbon) and 15 mg polytetrafluoroethylene (PTFE) were mixed in 10 mL ethanol for 4 h under stirring. Then, the mixture was air sprayed onto a Whatman separator (GF/A, No

Received: February 24, 2014
Accepted: July 9, 2014
Published: July 9, 2014

   dx.doi.org/10.1021/am5010943 | ACS Appl. Mater. Interfaces 2014, 6, 12083−12092

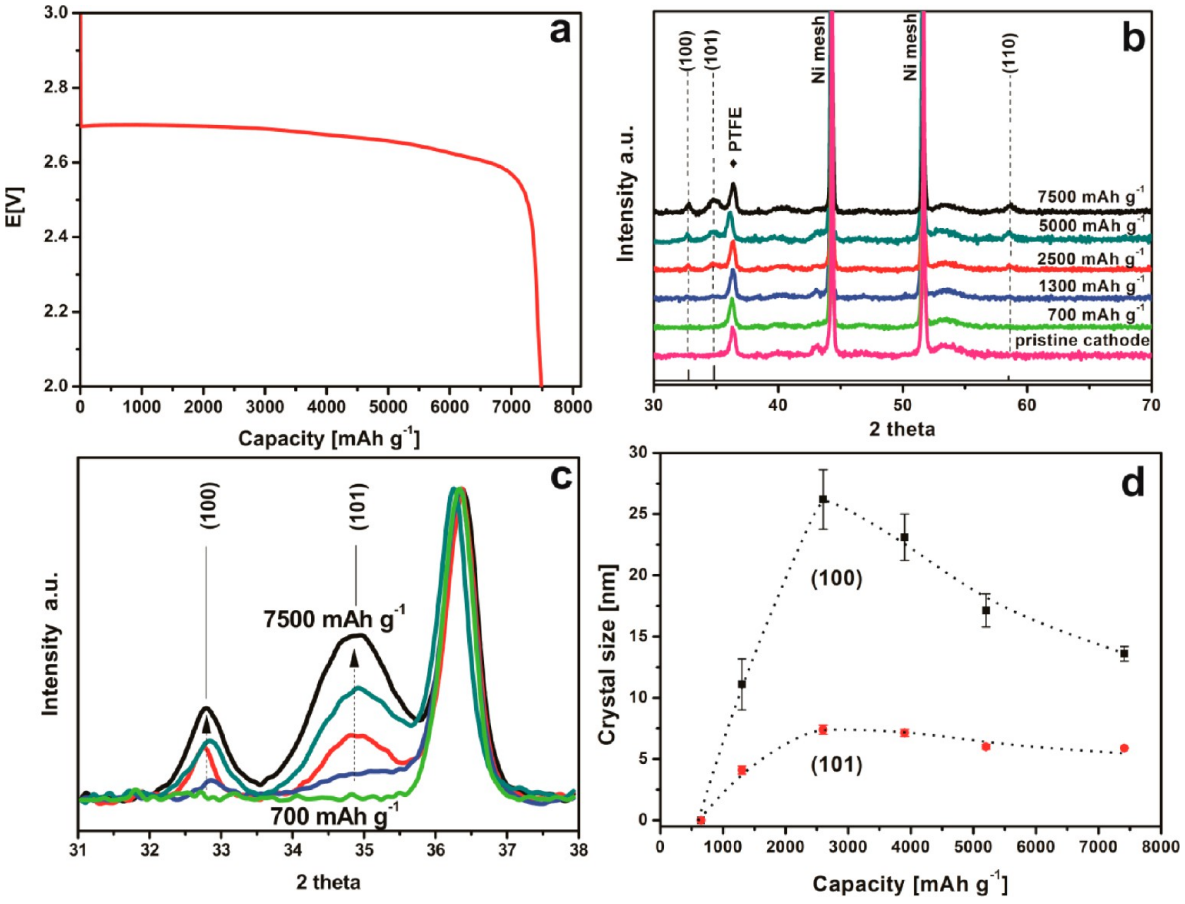

Figure 1. (a) First discharge voltage curve of a Li−O_2 cell at 0.1 mA cm^{-2}. (b) XRD patterns of a pristine cathode and cathodes discharged to different capacities. (c) XRD patterns of cathodes in (b) within the magnified 2θ range between 31° and 38° at a slow scan speed of 0.18° min^{-1}. (d) Variation of the crystal size of Li_2O_2 as a function of discharge capacity calculated from the (100) and (101) diffraction line profiles in (c).

1820−150) as support. The cathodes with a diameter of 10 mm (geometric area of 0.79 cm^2) were punched from the sprayed separator and then dried at 150 °C under vacuum overnight to remove all traces of moisture. The oxygen cathodes were then transferred into an argon-filled glovebox (< 1.0 ppm of H_2O and < 1.0 ppm of O_2) for cell assembly. All prepared cathodes had a typical carbon loading of 0.7 ± 0.1 mg cm^{-2} with a pore volume of 4.5 cm^3 g (carbon)$^{-1}$ determined by Brunauer−Emmett−Teller (BET) measurements.

Assembling Li−O_2 Cells. Lithium foil was used as anode and one piece of Celgard 2320 film soaked with 0.5 M lithium triflate in diglyme as electrolyte was applied as separator. The water content of electrolyte was below 10 ppm as determined by Karl Fischer titration. The carbon layer side of the cathode was exposed to the gas phase to improve the oxygen diffusion. During cell assembly, 60 μL of electrolyte was added to flood the cathode. Nickel Mesh was pressed on the carbon layer as current collector. After purging the cathode chamber for 30 s with oxygen flow under ambient pressure, the cell with a cathode chamber volume of 7 cm^3 was sealed for electrochemical testing at room temperature (conditioned climate) using a Maccor battery cycler. If not mentioned otherwise, a constant current density of 0.1 mA cm^{-2} was always used for discharge/charge while the cell potential was recorded simultaneously.

Characterization. Powder X-ray diffraction (XRD) was carried out using a X'Pert X-ray diffractometer with copper K-alpha (Philips PANalytical). XRD patterns of pristine cathodes were recorded in air while patterns of the discharged and charged cathodes after solvent washing were collected using a gastight sample holder to prevent reaction of Li_2O_2 with moisture and CO_2. Scanning electron microscope (SEM) images were taken to investigate the change of morphology of Li_2O_2 after discharge/charge to different depth using a MERLIN SEM from Zeiss NTS. The samples were transferred from the glovebox into the SEM with a gastight sample holder from Kammrath & Weiss. Raman measurements were performed using a Renishaw inVia Raman microscope system using an excitation wavelength of 633 nm. A gastight Linkam THMS600 variable temperature cell was used for the Raman measurements at −190 °C cooled by liquid nitrogen. Cyclic voltammetry (CV) of Li−O_2 cells with a Li reference electrode was performed using an EC-Lab (BioLogic SP300) at a slow scan rate of 0.1 mV s^{-1}.

RESULTS AND DISCUSSION

Characterization of Li_2O_2 Growth During ORR. Figure 1a shows the first discharge curve of a Li−O_2 cell discharged with a current density of 0.1 mA cm^{-2}. A typical discharge plateau is obtained starting at 2.7 V and then slowly decreasing to 2.6 V due to the increase of the thickness of insulating discharge products, i.e., mainly Li_2O_2. After discharge to a capacity of 7500 mAh g^{-1}, the cell voltage dropped quickly indicating the ceasing of the ORR reaction (a discharge voltage of 2 V was set as lower limit). The ex situ XRD measurements with a scan speed of 1.5° min^{-1} were carried out to identify the discharge products and study their crystal structure at different discharge depths as presented in Figure 1b. Below 1300 mAh g^{-1}, no distinct Li_2O_2 diffraction peaks were observed, likely due to the minor amount of crystalline Li_2O_2 formed at the initial discharge steps. When the discharge capacity was higher than 1300 mAh g^{-1}, three characteristic diffraction lines of Li_2O_2 appeared at 32°, 35°, and 58°.[14] With increasing discharge capacity, more Li_2O_2 was deposited in the cathode

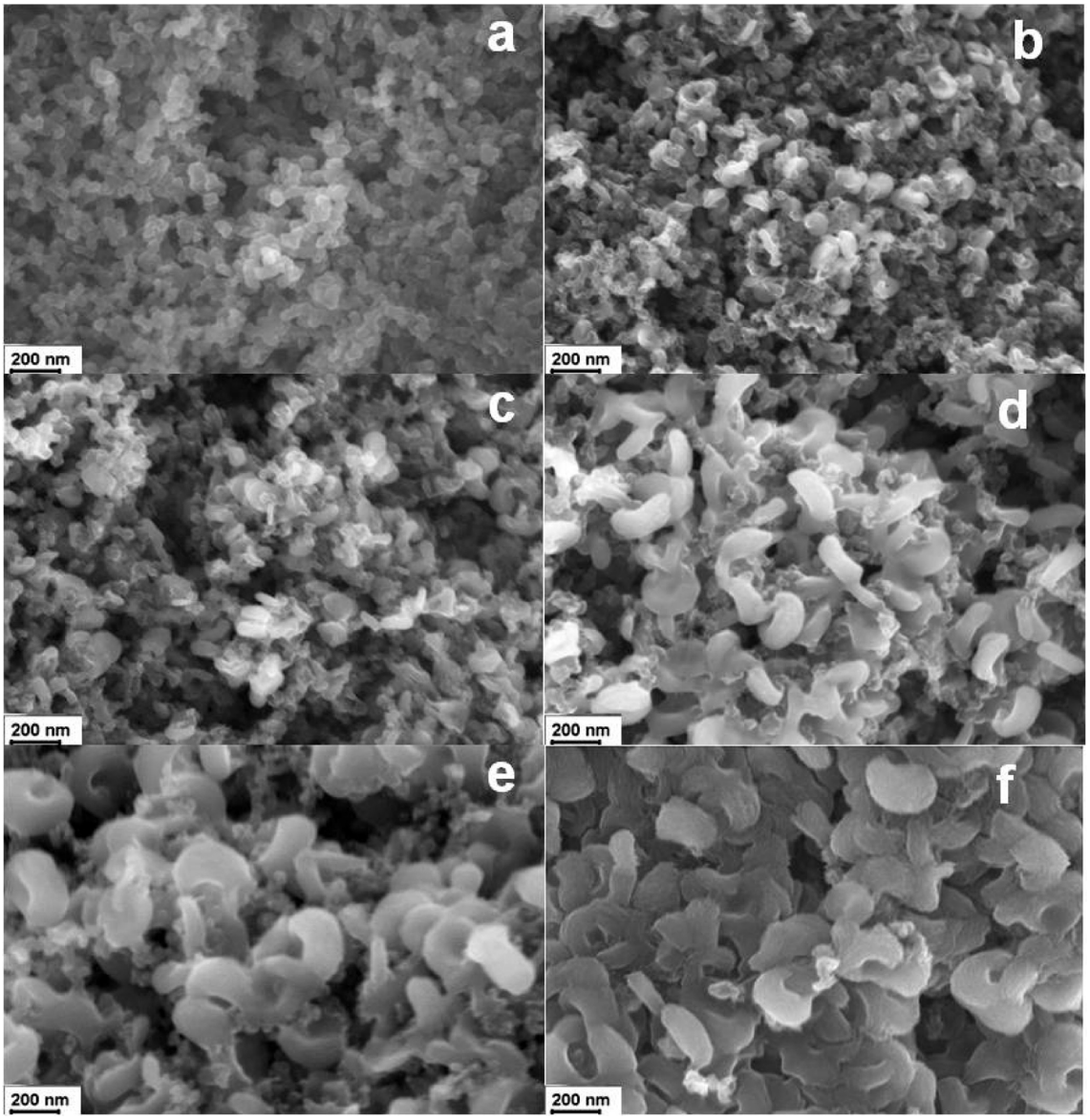

Figure 2. Morphology of Li_2O_2 products formed in the cathodes at different discharge capacities: (a) pristine cathode, (b) 250 mAh g^{-1}, (c) 1300 mAh g^{-1}, (d) 4000 mAh g^{-1}, (e) 5200 mAh g^{-1}, (f) 7500 mAh g^{-1}.

and thereby leading to an increase of the area of the Li_2O_2 diffraction peaks.[15] In order to obtain the crystal size of Li_2O_2 more precisely, the XRD patterns of discharged cathodes were recorded between 31° to 38° at a slower scan speed of 0.18° min^{-1} as shown in Figure 1c. The intensities of all peaks are normalized to the PTFE line at a peak central position of 36.5°. The crystal size of Li_2O_2 is evaluated by using the Scherrer equation based on the (100) and (101) planes, and the corresponding numbers should only be considered as estimates. As seen in Figure 1d, the nucleation and growth of Li_2O_2 during the initial discharge to a capacity of 2500 mAh g^{-1} leads to the increase of the crystal size up to 27 and 7 nm as determined from the (100) and (101) lattice planes, respectively. The significant difference of the crystal size as determined from the two reflections clearly indicates anisotropic growth of Li_2O_2 crystallites. Interestingly, both lengths decrease when the discharge proceeds and exceeds a discharge capacity of about 2500 mAh g^{-1}. At the end of discharge, the lengths have decreased to 14 and 5 nm, respectively. This unexpected decrease of the product crystal size during the ORR was also observed in in situ XRD studies of the Li−O_2 cell reaction.[16] Recently, it has been concluded from both experimental and theoretical studies that a superoxide-like phase is formed on the surface of Li_2O_2 during discharge.[17] The surface superoxide-like phase is likely to have a poor crystallinity, which may give rise to the apparently lower average crystal size of Li_2O_2.[18] More details on the investigation of the superoxide species will be given below.

The morphology of the Li_2O_2 products at different discharge depth are shown in the SEM images of Figure 2, and we can assess the morphological development. Before discharge, the pristine cathode composed of carbon nanoparticles with a diameter of 30 nm shows a highly porous structure as seen in Figure 2a. At low discharge capacities of 250 and 1300 mAh g^{-1}, many tiny disc-like nanoparticles appeared on the carbon surface as visible in Figure 2b and c. When the cell was discharged to 4000 mAh g^{-1}, the disc-like Li_2O_2 evolved to toroid-shaped particles growing upright in the cathode as

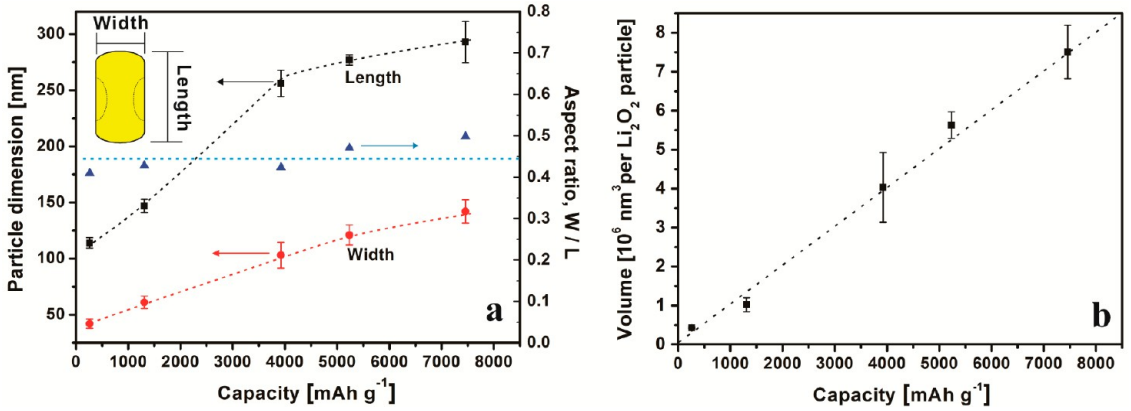

Figure 3. Effect of discharge capacity on particle dimension and aspect ratio (a) and the volume of single Li_2O_2 particles (b).

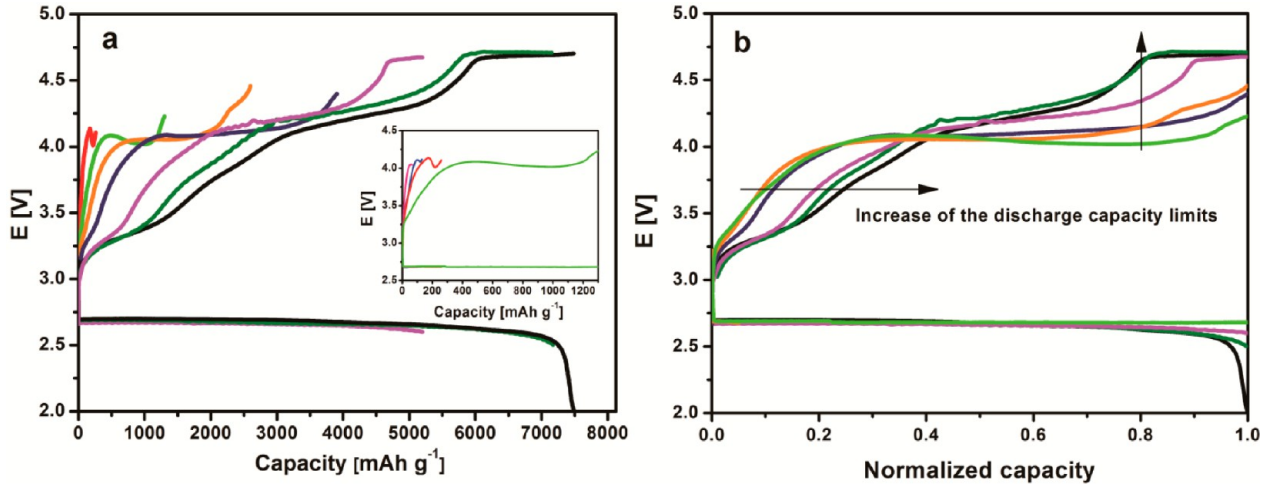

Figure 4. First discharge and charge profiles of Li−O_2 cells with different capacity limits (a) and scaled with normalized capacities (b) as abscissa, i.e., using the ratio of the specific capacity divided by the used discharge capacity limits in (a).

clearly seen in Figure 2d and e. These morphology changes of the discharge product are consistent with the results of Mitchell et al. when carbon nanotubes were used as cathode materials.[19] Toroids appear to represent the typical morphology of Li_2O_2 products formed in ether-based electrolytes,[20,21] and it was recently found by transmission electron microscopy (TEM) that these toroids consist of arrays of plate-like Li_2O_2 nanocrystallites.[19] Different hypotheses have been proposed to explain the observed toroid-shaped Li_2O_2 particles. Nazar speculated that the hexagonal crystal structure of Li_2O_2 and preferred nucleation on the prismatic crystal faces give rise to the formation of Li_2O_2 toroid aggregates.[22] In contrast, Shao-Horn attributed the unusual shape to plate splaying and secondary nucleation of additional plates.[19] Obviously, more work is needed to validate these hypotheses in detail. With prolonged discharge, Li_2O_2 nanotoroids grew continuously and finally covered the carbon surface completely as shown in Figure 2f. Known as pore-clogging effect, the growing Li_2O_2 gradually occupies the void volume of the porous carbon and finally blocks the oxygen diffusion path into the interior of the cathode resulting in the halt of the ORR.[23] Therefore, eliminating the pore clogging effect by optimizing 3D cathode microstructure or modifying the carbon surface by a structure promoter is critical to improve the discharge capacity of Li−O_2 cells.[10,24] On the other hand, with increasing current density, we found that both the discharge capacity and cell voltage decreased while the discharge products changed from the toroid-shaped particles composed of Li_2O_2 nanocrystallites into the (quasi) amorphous peroxide film (see Figure S1 in the Supporting Information). Nazar et al. attribute this variation of Li_2O_2 morphology and crystal structure to different reaction paths at elevated discharge rates.[17] At low discharge rate, the ORR follows a disproportionation mechanism forming several hundred nanometer-sized Li_2O_2 toroids caused by the LiO_2 solvation and surface nucleation of Li_2O_2. In contrast, a process of direct two-electron transfer governs the pathway at higher discharge rate limiting the thickness of Li_2O_2 film below 5 nm due to its low electrical conductivity. As shown in Figure S2 in the Supporting Information, during discharge to 2 V at a high current density of 1 mA cm^{-2}, no visible products were formed on the carbon cathode indicating that the limitation on discharge capacity has been turned from the pore clogging effect into carbon surface passivation which has been proven by atomic force microscopy (AFM) studies.[25] More investigations are also needed here to further reveal how the current density influences the kinetics of Li_2O_2 nucleation and growth and its related electrochemical properties.

In Figure 3a, the variation of the length (L) and width (W) of Li_2O_2 particles and their aspect ratio, defined as W/L, are shown as a function of the discharge capacity derived from the results in Figure 2. The length and width of the Li_2O_2 particles are 125 and 50 nm at an initial discharge capacity of 250 mAh

dx.doi.org/10.1021/am5010943 | ACS Appl. Mater. Interfaces 2014, 6, 12083−12092

g^{-1} and then increase to 275 and 130 nm at a discharge capacity of 5000 mAh g^{-1}. At the end of discharge, the values of length and width grow more slowly and finally reach 285 and 140 nm, respectively. The aspect ratio remains roughly constant in the range between 0.4 and 0.5 indicating uniform growth of Li_2O_2 particles. The volume change of a single Li_2O_2 particle during discharge is also calculated as presented in Figure 3b (more details on the geometric calculus are given in Figure S3 in the Supporting Information). The particle volume increases almost linearly with discharge capacity indicating that the ORR is the main electrochemical reaction as also proven by the XRD result in Figure 1.

Electrochemical Properties of Growing Li_2O_2 Products. In the next step we studied the electrochemical properties of Li_2O_2 products formed at different discharge capacities by comparing the charge profiles of the corresponding Li−O_2 cells. After defined discharge, the cells were recharged with the same charge to fully oxidize the formed Li_2O_2. When the discharge capacity was below 1300 mAh g^{-1} as shown in the inset graph of Figure 4a, the discharge voltage stabilized at 2.7 V. In contrast, the charge voltage rapidly increased up to 4.1 V and then decreased to 4 V which is the typical potential range for the oxidation of insulating Li_2O_2 in the absence of any catalysts, as widely reported in the literature.[26] Siegel et al. concluded from first-principles calculations that the bulk of Li_2O_2 crystallites is electrically insulating and that sufficient charge transport only occurs at moderately high charging voltages (i.e., typically above 4 V) that drive partial delithiation and lead to the formation of mobile polaron-type electronic holes.[27] Moreover, a recent study on Tafel plots of cathodes in Li−O_2 cells also proved that the considerably large overpotential originates from the cell impedance rather than surface kinetics.[28] The resulting high charge overpotential (>1 V) causes a low energy efficiency and—more important—the instability of the electrolyte which finally limits the cycling performance of cells.[29] Therefore, the improvement of the charge transfer to Li_2O_2, e.g., by using a redox mediator, will be crucial to achieve sufficiently rechargeable Li−O_2 batteries.[30] On charge, the gradual oxidation of insulating Li_2O_2 lowers the resistance of the cathode leading to a slow decrease of the charge overvoltage. At the end of charge the cell voltage increased slightly indicating that a small amount of Li_2O_2 products has been chemically consumed by side reactions resulting in the loss of reversible capacity. This observation is also consistent with reports in the literature that Li_2O_2 shows chemical reactivity toward both carbon and electrolyte.[12,31] Here, the charge behavior above 4 V dominates the charge profile suggesting that the Li_2O_2 nanodiscs (see the SEM images in Figure 2) formed at a low discharge capacity mainly show bulk behavior, i.e., the poor conductivity of Li_2O_2 bulk causing the high charge overpotential.

With proceeding discharge to a capacity of 2500 mAh g^{-1} as shown in Figure 4a, a long charge plateau at a voltage of 4.1 V is observed due to the growth of disc-shaped Li_2O_2 particles as shown in Figure 2c, forming more insulating Li_2O_2 for oxidation. Meanwhile, prior to bulk decomposition, a sloping charge profile at a lower charge voltage between 3.3 to 4.1 V becomes more pronounced. Shao-Horn et al. suggest that the charge process in this sloping region is controlled by the surface properties of Li_2O_2 particles, which thus corresponds to the oxidation of the particle surface.[32] Different from the insulating Li_2O_2 bulk, the facets of Li_2O_2 crystallites have been computed to be (half) metallic and thereby present a much lower theoretical charge overpotential than the intrinsically insulating Li_2O_2 bulk as suggested by the results obtained from density functional theory calculations (DFT).[33] Consistent with it, when the discharge capacity is higher than 1300 mAh g^{-1}, Li_2O_2 crystallites are formed as proven by XRD results in Figure 1. We speculate that the crystalline Li_2O_2 shells are formed above 2500 mAh g^{-1}covering the initially formed cores. Upon charge, the gradual consumption of conducting Li_2O_2 shells probably lowers the conductance giving a slope-like charge profile followed by the oxidation of Li_2O_2 cores with insulating bulk property giving a charge plateau at 4.1 V (see Figure S4 in the Supporting Information).

When the discharge capacity is higher than 4000 mAh g^{-1} (cell voltage decreased below 2.65 V), additionally a short charge plateau appeared at a lower voltage of about 3 to 3.4 V. In conjunction, another charge plateau as high as 4.75 V appeared, which is the typical potential for decomposition of ether-based electrolytes (see Figure S5 in the Supporting Information), and which indicates a significant loss of reversible discharge products. Consistent with this, higher fractions of charge capacity are achieved above 4.2 V at deeper discharge as shown in Figure 4b. However, no references, so far, reported that any side products of Li−O_2 cells could be electrochemically decomposed below 3.4 V. The main side products, e.g., Li_2CO_3 and LiOH, are not rechargeable within the reasonable potential range as shown in Supporting Information Figure S5 and reported in the literature.[25] In addition, as shown in Figure 2, the Li_2O_2 discs evolved to the toroidal particles when the discharge capacity was higher than 4000 mAh g^{-1}. The surfaces and sides of Li_2O_2 discs likely developed to the indentations and rims of Li_2O_2 toroids, respectively, as proposed in the recent literature.[19] Therefore, we speculate that a LiO_x phase with a comparably high electronic conductivity is formed on the rims of Li_2O_2 toroids with large surface area. When the charge voltage reaches 3.4 V, the rims of Li_2O_2 toroids disappear causing the degradation of the Li_2O_2 toroids to Li_2O_2 discs as seen in Supporting Information Figure S4. This assumption is also consistent with recent conclusions by Yang et al. that a superoxide-like component is formed on the surface of peroxide as confirmed by low temperature Raman spectra and magnetic measurements.[17] The oxidation of a superoxide-like component was proposed to give rise to such a low voltage charge plateau.[34] The nucleophilic attack of the formed superoxide-like phase toward the electrolyte and the resulting side products, e.g., Li_2CO_3 as confirmed by infrared spectroscopy (IR) (see Figure S6 in the Supporting Information), also would explain the significant loss of reversible discharge products as shown in Figure 4. Consistent with this conclusion, Nazar et al. found a drastic 30-fold increase in the carbonate content of a cathode charged at 3.4 V by time-of-flight secondary ion mass spectrometry (ToF-SIMS) while much less carbonate was formed at higher potentials during Li_2O_2 oxidation, i.e., around 4 V.[35] McCloskey et al. also reported that carbonate formation during the initial charging stage originates from the LiO_2 (or Li_2O_2) induced electrolyte decomposition, which ultimately evolves CO_2 at high charge potential of 4−4.5 V.[12] Based on our experimental results, a hypothetical charge mechanism is proposed as shown in Figure S7 in the Supporting Information.

The Li−O_2 cells used for the experiments shown in Figure 4 were further cycled to evaluate the effect of the depth of discharge (DoD) on the cycle stability of cells as shown in Figure 5. The maximal cycling number of the cells was recorded once the charge voltage achieved 4.5 V, although the cells can

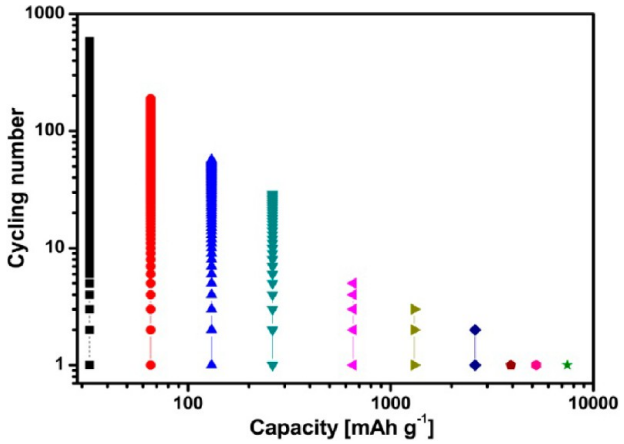

Figure 5. Effect of discharge capacity on the cycle life of Li−O_2 cells.

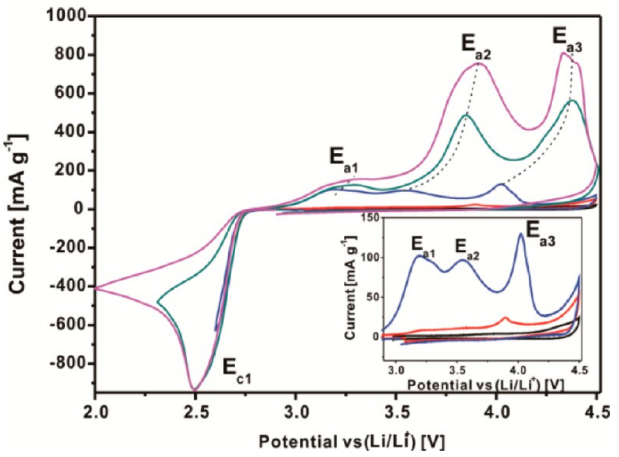

Figure 6. Cyclic voltammograms of cathodes in Li−O_2 cells using 0.5 M $LiSO_3CF_3$/diglyme electrolyte with varied cathodic potential limits at a slow scan rate of 0.1 mV s^{-1}. The upper anodic potential is set at 4.5 V.

be further cycled. At a very low discharge capacity of 35 mAh g^{-1}, the cell could be cycled for about 600 times. However, the cycling number already decreases significantly down to 60 at a discharge capacity of 130 mAh g^{-1}. When the discharge capacity was adjusted to values higher than 4000 mAh g^{-1}, the cells could be cycled only once. Moreover, cells discharged at lower capacity do not only show larger cycling numbers but also a higher cumulative capacity as presented in Figure S8 in the Supporting Information. Thus, the cycling stability of Li−O_2 cells is indeed improved by "limited discharge steps" as widely reported in the literature.[36] However, as the relation between the maximum cycle number and DoD is clearly nonlinear, the degradation of the cells is probably caused by different mechanisms depending on the DoD. Recently, it has been reported that Li_2O_2 chemically degrades glyme solvents into carboxylate containing species on the Li_2O_2/electrolyte interface as proven by X-ray photoelectron spectroscopy (XPS).[37] McCloskey et al. found by differential electrochemical mass spectrometry (DEMS) that Li_2O_2-induced electrolyte instability (including solvent and salt) accounts for nearly all efficiency loss during limited discharge.[38] They conclude that Li_2O_2 might react with various electrolytes by either nucleophilic attack or α/β-hydrogen abstraction. Thus, the growth of Li_2O_2 particles during discharge increases the Li_2O_2/electrolyte interface area where the parasitic reactions take place and thereby gradually lowers the cycling number. When the discharge capacity is larger than 4000 mAh g^{-1}, the cells rapidly degrade in one cycle due to the formation of a surface superoxide-like phase as described before, which indicates that superoxide shows higher chemical reactivity than peroxide as suggested by experiments using an electrochemical quartz crystal microbalance (EQCM).[39]

The effect of cathodic potential limits on the cyclic voltammograms of the carbon cathode in Li−O_2 cells is displayed in Figure 6. The upper anodic potential is always set at 4.5 V ensuring full decomposition of Li_2O_2.[40] One distinct reduction peak, E_{c1}, is observed with an onset potential at 2.75 V while three oxidation peaks, i.e., E_{a1}, E_{a2}, and E_{a3}, appear in the anodic domain. On the basis of CV and rotating disk electrode (RDE) studies,[41,42] Laoire et al. concluded that the single reduction peak is due to a one-electron transfer process, i.e., oxygen reduction forming LiO_2 (eq 1). Then, LiO_2 chemically disproportionates into Li_2O_2 and O_2 (eq 2) causing the irreversible electrochemical pathway of the ORR.

$$Li^+ + O_2 + e^- = LiO_2 \qquad (E_{c1}) \tag{1}$$

$$2LiO_2 = Li_2O_2 + O_2 \tag{2}$$

As shown in Figure 6, the number and the size of the oxidation peaks are found to depend on the cathodic limits. With only anodic polarization as shown in the black curve of the inset graph, the electrochemical decomposition of diglyme begins at 4.2 V. When the cathodic potential is swept first to 2.7 V (red curve), only a single oxidation peak is observed between 3.8 and 4.1 V. This potential range agrees well with the galvanostatic experiments (in Figure 4), i.e., the oxidation of Li_2O_2 cores with insulating bulk property (eq 3) formed in the initial discharge process.

$$Li_2O_2(\text{core}) = 2Li^+ + O_2 + 2e^- \qquad (E_{a3}) \tag{3}$$

In contrast, when the cathodic potential limit was set to 2.6 V (blue curve), this bulk oxidation peak grows and shifts to higher anodic potential while the peak of electrolyte decomposition above 4.2 V increases as well. More interesting, two partially overlapping oxidation peaks appear at lower peak potentials of 3.2 and 3.6 V. The potential range of these two peaks is quite close to the range of the low charge voltage plateau and sloping profile as shown in Figure 4, and thus probably corresponds to the oxidation of the surface superoxide-like phase (eq 4) and Li_2O_2 shells (eq 5), respectively.

$$O_2^- = O_2 + e^- \qquad (E_{a1}) \tag{4}$$

$$Li_2O_2(\text{shell}) = 2Li^+ + O_2 + 2e^- \qquad (E_{a2}) \tag{5}$$

Although eqs 3 and 5 represent chemically the same reaction, the different conductivities of Li_2O_2 cores and shells result in the different oxidation potential domains. It is worth noting that the charge reactions in eqs 3−5 may include one or multiple steps as proposed in the literature.[43−45] More studies are needed to clarify the complex charge mechanism. With the cathodic potential limit decreased to 2 V, all three oxidation peaks expand and shift toward higher potential due to more poorly conducting discharge products being formed. Consistent with the conclusion in Figure 4, the discharge depth (or overpotential) determines the composition of discharge

products and thereby influences the charge/oxidation behaviors of cathode.

Superoxide-Like Species on the Surface of Li_2O_2. After being fully discharged to 2 V under galvanostatic conditions with 0.1 mA cm^{-2}, the carbon cathodes were washed and sealed under Ar for the characterization by Raman spectroscopy. To enhance the Raman intensity of the discharge products, the measurements were carried out at −190 °C cooled by liquid nitrogen. The D band from Ketjenblack carbon material gives a distinct peak at a wavenumber of about 1000−1500 cm^{-1} as shown in Figure S9 in the Supporting Information and partially seen in Figure 7.

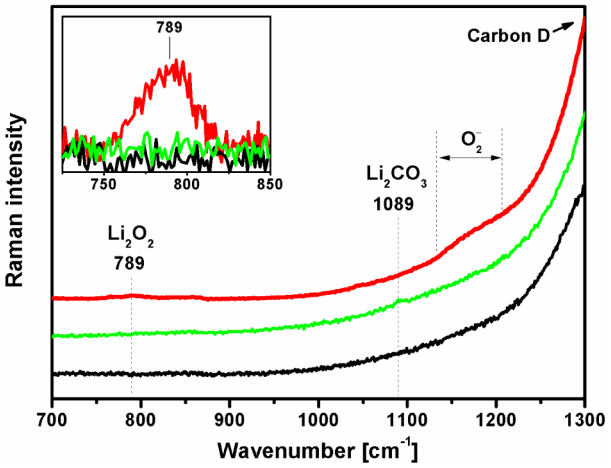

Figure 7. Raman spectrum of the pristine cathode (black) and fully discharged cathodes with (green) and without (red) exposure to air measured at −190 °C.

Compared to the pristine cathode (black curve) in Figure 7, the fully discharged cathode (red curve) presents a small peak at 789 cm^{-1} as shown in the inset graph which indicates the formation of Li_2O_2 consistent with XRD results in Figure 1. More interesting, a very small and broad shoulder is observed between 1130 and 1200 cm^{-1}. Signals in this wavenumber range may originate from O_2^- like stretch vibrations, e.g., the Raman signal at 1156 cm^{-1} in sodium superoxide (NaO_2),[46] which is also consistent with the reported O−O stretch of LiO_2 at 1137 cm^{-1} measured by surface enhanced Raman spectroscopy (SERS).[45] The position and range of this shoulder fit well with the frequency of the superoxide-like species simulated by Amine et al. as part of the surface structure of Li_2O_2 particles (~1150 cm^{-1} to 1190 cm^{-1}).[17] Meanwhile, Shao-Horn et al. reported that the oxygen anions on the dominating O-rich (0001) face of Li_2O_2 crystallites are arranged in a LiO_2-like electronic structure as proven by its X-ray absorption near edge structure (XANES) and as predicted by computational studies.[32] Here, the broad shoulder with low intensity in the Raman spectrum probably indicates that the formed superoxide-like phase shows large O-rich (0001) facets with poor crystallinity, which could also explain the decrease of crystalline size at deeper discharge as shown in the XRD results (Figure 1). We propose that many point defects (e.g., electronic holes due to lithium deficiency) probably exist on the O-rich (0001) facets resulting in the poor crystallinity and high conductivity of superoxide-like phase. Consistent with that, Merkle et al. also assumed a surface-defective peroxide phase due to an enhanced signal in electron paramagnetic resonance (EPR) from a ball milled Li_2O_2 sample with 1 order of magnitude increase in the electronic conductivity.[47] Yilmaz et al. observed that a noncrystalline Li_2O_2 thin layer presented a low charge overpotential (~3.5 V) probably due to the high conductivity of the defective Li_2O_2 products.[48] These experimental observations indicate that the superoxide-like phase, which is also supported by our current results, probably exists as defective Li_2O_2 phase rather than thermodynamically unstable bulk LiO_2.[49] However, more studies are needed to determine the surface defects and conductivity. After exposure to air for 15 min, this shoulder disappeared as shown by the green curve, and instead a small Li_2CO_3 peak appeared at 1089 cm^{-1}, probably caused by reaction with CO_2 present in air. In addition, this observation proves that the shoulder observed in the Raman spectra represents a reactive surface of discharge products formed upon discharge rather than the residual electrolyte and air-stable side products, e.g., organic Li compounds and surface groups of carbon.

To further investigate the surface superoxide-like species, the Li−O_2 cells were discharged at different current densities followed by charging at a constant current density of 0.1 mA cm^{-2}. Both the discharge and charge capacities were kept at 2500 mAh g^{-1} for all cells. When the discharge current density was increased from 0.1 to 0.2 mA cm^{-2}, the discharge voltage decreased from 2.7 to 2.65 V due to the polarization effect, as shown in Figure 8. More interesting, it shortened the charge

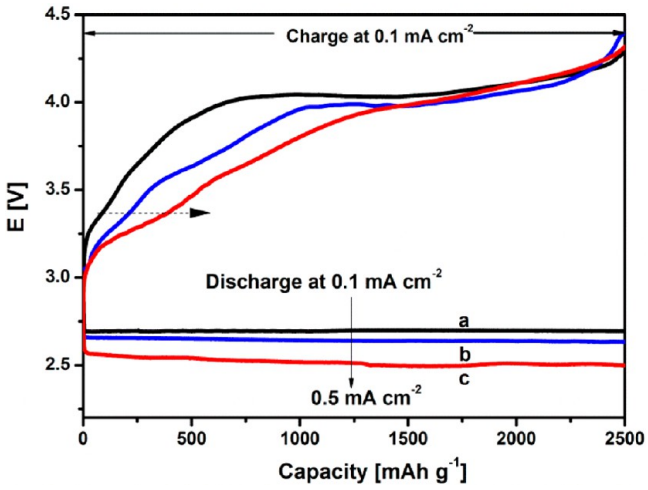

Figure 8. Influence of different discharge currents on the discharge and charge profiles of Li−O_2 cells with a constant capacity of 2500 mAh g^{-1}. (a) 0.1 mA cm^{-2} (b) 0.2 mA cm^{-2}, and (c) 0.5 mA cm^{-2}.

plateau of Li_2O_2 bulk oxidation at around 4 V compensated with a plateau-like charge behavior below 3.5 V. At a discharge current density of 0.5 mA cm^{-2}, the discharge voltage was further decreased to 2.5 V. The low-voltage charge plateau appears again as the one observed in Figure 4. Here, it indicates that the formation of superoxide-like phase is likely potential dependent rather than capacity dependent (here always 2500 mAh g^{-1}) consistent with the CV results in Figure 6. When the discharge potential is lower than 2.65 V, the formation of O-rich (0001) facets of Li_2O_2 with superoxide-like character is thermodynamically preferred to other (non)stoichiometric facets due to its lower surface energy as calculated by Hummelshøj.[50] Therefore, controlling the discharge overpotential to avoid the formation of defective facets with high

chemical reactivity in Li_2O_2 products is an alternative way to improve the cycling performance of Li−O_2 cells.

Hypothesis on the Growth Mechanisms of Core−Shell Li_2O_2 Particles during Discharge. According to the experimental results presented in this work, we hypothesize a growth mechanism of Li_2O_2 particles during discharge as depicted in Figure 9. At low discharge capacity below 1300 mAh g^{-1} (region I), Li_2O_2 deposits on the surface of carbon forming Li_2O_2 cores as marked in yellow. These disc-shaped Li_2O_2 nanocores present insulating bulk properties causing a high charge potential above 4 V. Upon further discharge to 4000 mAh g^{-1} (region II), more Li_2O_2 nucleates on the nucleation sites of Li_2O_2 nanocores leading to the increase of disc sizes and formation of crystalline Li_2O_2 shells. These crystalline Li_2O_2 shells (as marked in blue) are electrically conductive exhibiting a slope-like charge behavior below 4.1 V. When the discharge capacity is higher than 4000 mAh g^{-1} (discharge voltage decreases below 2.65 V), a defective superoxide-like phase is formed on the rims of Li_2O_2 nanodiscs as marked in red (region III). The contained defects (as marked as black dots) may act as the preferred nucleation sites for particle growth controlling the morphological development of Li_2O_2 from disc- to toroid-shaped particles. Meanwhile, the defective phase probably has high conductivity giving a charge plateau below 3.4 V, whereas its high chemical reactivity degrades the stability of cells rapidly. Further studies are needed to examine this hypothesis in detail.

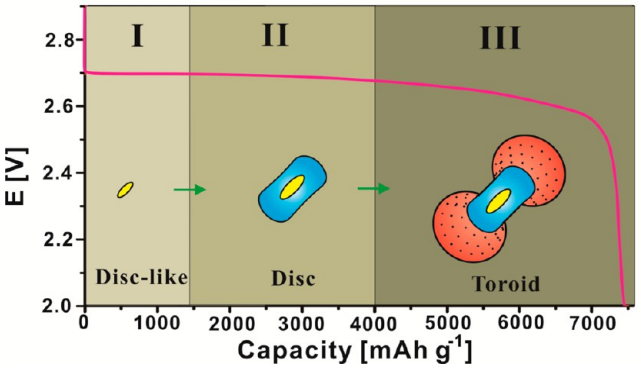

Figure 9. Schematic illustration of the proposed Li_2O_2 growth mechanism. The cross sections of Li_2O_2 particles are given in the figure reflecting the shape evolution during discharge.

CONCLUSIONS

In this work, the evolution of Li_2O_2 growth during discharge was investigated to reveal its effect on the kinetics of Li−O_2 batteries. The physical and chemical properties of the Li_2O_2 deposits depend strongly on the discharge depth and overpotentials. Within the initial discharge stage, the formed Li_2O_2 cores with disc-like shapes mainly show insulating bulk conductivity giving a high charge voltage at 4.1 V. With the nucleation and growth of Li_2O_2 crystallites at higher discharge capacity, the electrically conducting Li_2O_2 shells are formed covering the cores leading to a sloping charge behavior at a lower voltage range of 3.3 to 4.1 V. When the voltage was decreased below 2.65 V in a deep discharge step, the Li_2O_2 discs evolved to the characteristic Li_2O_2 toroids, while the defective superoxide-structured phase with high conductivity was formed on the rims of Li_2O_2 toroids causing a comparably low charge plateau below 3.4 V. Both Li_2O_2 and the superoxide-like phase appear to be unstable in ether-based electrolytes resulting in the degradation of cells. However, this study also points out that the reversibility of Li−O_2 batteries can be enhanced by controlling the growth of Li_2O_2 to tune its chemical reactivity.

ASSOCIATED CONTENT

Supporting Information

Effect of current density on performance of Li−O_2 cells, calculation of the volume of a single Li_2O_2 particle, morphology and crystalline structure of the Li_2O_2 products at different charge depth, examination of the chargeability of LiOH and Li_2CO_3, infrared spectrum of cathode fully discharged to 2 V, a proposed reaction mechanism of Li_2O_2 oxidation, effect of discharge depth on the accumulative discharge capacity of Li−O_2 cells during cycling, Raman spectrum of carbon cathode fully discharged to 2 V. This material is available free of charge via the Internet at http://pubs.acs.org.

AUTHOR INFORMATION

Corresponding Authors

*E-mail: Chun.Xia@phys.chemie.uni-giessen.de.
*E-mail: juergen.janek@phys.chemie.uni-giessen.de.

Notes

The authors declare no competing financial interest.

ACKNOWLEDGMENTS

This study was part of the project of "High Energy Lithium Ion Battery (HE-Lion)" under the innovation alliance of "Lithium Ion Battery (LIB2015)" funded by the German Federal Ministry of Education and Research (BMBF). Support by the state of Hessen (Laboratory for Materials Research, ElCh platform) and the Store-E project (LOEWE Program, State of Hessen) are also acknowledged. We thank P. Hartmann and P. Adelhelm for fruitful discussions.

REFERENCES

(1) Abraham, K. M.; Jiang, Z. Polymer Electrolyte-Based Rechargeable Lithium/Oxygen Battery. *J. Electrochem. Soc.* **1996**, *143*, 1−5.
(2) Christensen, J.; Albertus, P.; Sanchez-Carrera Roel, S.; Lohmann, T.; Kozinsky, B.; Liedtke, R.; Ahmed, J.; Kojica, A. A Critical Review of Li/Air Batteries. *J. Electrochem. Soc.* **2012**, *159*, R1−R30.
(3) Balaish, M.; Kraytsberg, A.; Ein-Eli, Y. A Critical Review on Lithium−Air Battery Electrolytes. *Phys. Chem. Chem. Phys.* **2014**, *16*, 2801−2822.
(4) Padury, R.; Zhang, X. W. Lithium−Oxygen Batteries—Limiting Factors that Affect Performance. *J. Power Sources* **2011**, *196*, 4436−4444.
(5) Hartmann, P.; Bender, C.; Vračar, M.; Dürr, A. K.; Garsuch, A.; Janek, J.; Adelhelm, P. A Rechargeable Room-temperature Sodium Superoxide (NaO_2) Battery. *Nat. Mater.* **2013**, *12*, 228−232.
(6) Débart, A.; Paterson, A. J.; Bao, J. L.; Bruce, P. G. Alpha-MnO_2 Nanowires: a Catalyst for the O_2 Electrode in Rechargeable Lithium Batteries. *Angew. Chem., Int. Ed.* **2008**, *47*, 4521−4524.
(7) Lu, Y. C.; Xu, Z. C.; Gasteiger, H. A.; Chen, S.; Hamad-Schifferli, K.; Sao-Horn, Y. Platinum−Gold Nanoparticles: A Highly Active Bifunctional Electrocatalyst for Rechargeable Lithium−Air Batteries. *J. Am. Chem. Soc.* **2010**, *132*, 12170−12171.
(8) Garsuch, A.; Badine, D. M.; Leitner, K.; Gasparotto, L. H. S.; Borisenko, N.; Endres, F.; Vračar, M.; Janek, J.; Oesten, R. Investigation of Various Ionic Liquids and Catalyst Materials for Lihium-Oxygen Batteries. *Z. Phys. Chem.* **2012**, *226*, 107−119.

(9) Harding, J. R.; Lu, Y. C.; Tsukada, Y.; Shao-Horn, Y. Evidence of Catalyzed Oxidation of Li_2O_2 for Rechargeable Li–Air Battery Applications. *Phys. Chem. Chem. Phys.* **2012**, *14*, 10540–10546.
(10) Xia, C.; Waletzko, M.; Peppler, K.; Janek, J. Silica Nanoparticles as Structural Promoters for Oxygen Cathodes of Lithium–Oxygen Batteries. *J. Phys. Chem. C* **2013**, *117*, 19897–19904.
(11) Viswanathan, V.; Thygesen, K. S.; Hummelshøj, J. S.; Nørskov, J. K.; Girishkumar, G.; McCloskey, B. D.; Luntz, A. C. Electrical Conductivity in Li_2O_2 and Its Role in Determining Capacity Limitations in Non-aqueous Li-O_2 Batteries. *J. Chem. Phys.* **2011**, *135*, (214704)1–10.
(12) McCloskey, B. D.; Speidel, A.; Scheffler, R.; Miller, D. C.; Viswanathan, V.; Hummelshøj, J. S.; Nørskov, J. K.; Luntz, A. C. Twin Problems of Interfacial Carbonate Formation in Nonaqueous Li–O_2 Batteries. *J. Phys. Chem. Lett.* **2012**, *3*, 997–1001.
(13) Wang, Y. G.; Xia, Y. Y. Li–O_2 Batteries: An Agent for Change. *Nat. Chem.* **2013**, *5*, 445–447.
(14) Freunberger, S. A.; Chen, Y. H.; Drewett, N. E.; Hardwick, L. J.; Bard, F.; Bruce, P. G. The Lithium-Oxygen battery with Ether-based Electrolyte. *Angew. Chem., Int. Ed.* **2011**, *50*, 8609–8613.
(15) Shui, J. L.; Okasinski, J. S.; Chen, C.; Almer, J. D.; Liu, D. J. In Operando Spatiotemporal Study of Li_2O_2 Grain Growth and its Distribution Inside Operating Li–O_2 Batteries. *ChemSusChem* **2014**, *7*, 543–548.
(16) Lim, H.; Yilmaz, E.; Byon, H. R. Real-Time XRD Studies of Li–O_2 Electrochemical Reaction in Nonaqueous Lithium–Oxygen Battery. *J. Phys. Chem. Lett.* **2012**, *3*, 3210–3215.
(17) Yang, J. B.; Zhai, D. Y.; Wang, H. H.; Lau, K. C.; Schlueter, J. A.; Du, P.; Myers, D. J.; Sun, Y. K.; Curtiss, L. A.; Amine, K. Evidence for Lithium Superoxide-Like Species in the Discharge Product of a Li–O_2 Battery. *Phys. Chem. Chem. Phys.* **2013**, *15*, 3764–3771.
(18) Adams, B. D.; Radtke, C.; Black, R.; Trudeau, M. L.; Zaghib, K.; Nazar, L. F. Current Density Dependence of Peroxide Formation in the Li–O_2 Battery and Its Effect on Charge. *Energy Environ. Sci.* **2013**, *6*, 1772–1778.
(19) Mitchell, R. R.; Gallant, B. M.; Shao-Horn, Y.; Thompson, C. V. Mechanisms of Morphological Evolution of Li_2O_2 Particles during Electrochemical Growth. *J. Phys. Chem. Lett.* **2013**, *4*, 1060–1064.
(20) Xia, C.; Bender, C. L.; Bergner, B.; Peppler, K.; Janek, J. An Electrolyte Partially-Wetted Cathode Improving Oxygen Diffusion in Cathodes of Non-Aqueous Li-Air Batteries. *Electrochem. Commun.* **2013**, *26*, 93–96.
(21) Fan, W.; Cui, Z.; Guo, X. Tracking Formation and Decomposition of Abacus-Ball-Shaped Lithium Peroxides in Li–O_2 Cells. *J. Phys. Chem. C* **2013**, *117*, 2623–2627.
(22) Black, R.; Oh, S. H.; Lee, J. H.; Yim, T.; Adams, B.; Nazar, L. F. Screening for Superoxide Reactivity in Li-O_2 Batteries: Effect on Li_2O_2/LiOH Crystallization. *J. Am. Chem. Soc.* **2012**, *134*, 2902–2905.
(23) Read, J. Characterization of the Lithium/Oxygen Organic Electrolyte Battery. *J. Electrochem. Soc.* **2002**, *149*, A1190–A1195.
(24) Xiao, J.; Mei, D.; Li, X.; Xu, W.; Wang, D.; Graff, G. L.; Bennett, W. D.; Nie, Z.; Saraf, L. V.; Aksay, I. A.; Liu, J.; Zhang, J. G. Hierarchically Porous Graphene as a Lithium-Air Battery Electrode. *Nano Lett.* **2011**, *11*, 5071–5078.
(25) Wen, R.; Hong, M.; Byon, H. R. In Situ AFM Imaging of Li-O_2 Electrochemical Reaction on Highly Oriented Pyrolytic Graphite with Ether-Based Electrolyte. *J. Am. Chem. Soc.* **2013**, *135*, 10870–10876.
(26) Meini, S.; Tsiouvaras, N.; Schwenke, K. U.; Piana, M.; Beyer, H.; Lange, L.; Gasteiger, H. A. Rechargeability of Li–Air Cathodes Pre-filled with Discharge Products Using an Ether-Based Electrolyte Solution: Implications for Cycle-Life of Li–Air Cells. *Phys. Chem. Chem. Phys.* **2013**, *15*, 11478–11493 30.
(27) Radin, M. D.; Siegel, D. J. Charge Transport in Lithium Peroxide: Relevance for Rechargeable Metal–Air Batteries. *Energy Environ. Sci.* **2013**, *6*, 2370–2379.
(28) Viswanathan, V.; Nørskov, J. K.; Speidel, A.; Scheffler, R.; Gowda, S.; Luntz, A. C. Li–O_2 Kinetic Overpotentials: Tafel Plots from Experiment and First Principles Theory. *J. Phys. Chem. Lett.* **2013**, *4*, 556–560.
(29) Guo, X. X.; Zhao, N. The Role of Charge Reactions in Cyclability of Lithium–Oxygen Batteries. *Adv. Energy Mater.* **2013**, *3*, 1413–1416.
(30) Chen, Y. H.; Freunberger, S. A.; Peng, Z. Q.; Fontaine, O.; Bruce, P. G. Charging a Li–O_2 Battery Using a Redox Mediator. *Nat. Chem.* **2013**, *5*, 489–494.
(31) Gowda, S. R.; Brunet, A.; Wallraff, G. M.; McCloskey, B. D. Implications of CO_2 Contamination in Rechargeable Nonaqueous Li–O_2 Batteries. *J. Phys. Chem. Lett.* **2013**, *4*, 276–279.
(32) Gallant, B. M.; Kwabi, D. G.; Mitchell, R. R.; Zhou, J. G.; Thompson, C. V.; Shao-Horn, Y. Influence of Li_2O_2 Morphology on Oxygen Reduction and Evolution Kinetics in Li–O_2 Batteries. *Energy Environ. Sci.* **2013**, *6*, 2518–2528.
(33) Radin, M. D.; Rodriguez, J. F.; Tian, F.; Siegel, D. J. Lithium Peroxide Surfaces Are Metallic, While Lithium Oxide Surfaces. *J. Am. Chem. Soc.* **2012**, *134*, 1093–1103.
(34) Zhai, D. Y.; Wang, H. H.; Yang, J. B.; Lau, K. C.; Li, K. X.; Amine, K.; Curtiss, L. A. Disproportionation in Li–O_2 Batteries Based on a Large Surface Area Carbon Cathode. *J. Am. Chem. Soc.* **2013**, *135*, 15364–15372.
(35) Black, R.; Lee, J. H.; Adams, B.; Mims, C. A.; Nazar, L. F. The Role of Catalysts and Peroxide Oxidation in Lithium–Oxygen Batteries. *Angew. Chem., Int. Ed.* **2013**, *52*, 392–396.
(36) Laoire, C.; Mukerjee, S.; Plichta, E. J.; Hendrickson, M. A.; Abraham, K. M. Rechargeable Lithium/TEGDME-LiPF_6/O_2 Battery. *J. Electrochem. Soc.* **2011**, *158*, A302–A308.
(37) Younesi, R.; Hahlin, M.; Björefors, F.; Johansson, P.; Edström, K. Li–O_2 Battery Degradation by Lithium Peroxide (Li_2O_2): A Model Study. *Chem. Mater.* **2013**, *25*, 77–84.
(38) McCloskey, B. D.; Valery, A.; Luntz, A. C.; Gowda, S. R.; Wallraff, G. M.; Garcia, J. M.; Mori, T.; Krupp, L. E. Combining Accurate O_2 and Li_2O_2 Assays to Separate Discharge and Charge Stability Limitations in Nonaqueous Li–O_2 Batteries. *J. Phys. Chem. Lett.* **2013**, *4*, 2989–2993.
(39) Sharon, D.; Etacheri, V.; Garsuch, A.; Afri, M.; Frimer, A. A.; Aurbach, D. On the Challenge of Electrolyte Solutions for Li–Air Batteries: Monitoring Oxygen Reduction and Related Reactions in Polyether Solutions by Spectroscopy and EQCM. *J. Phys. Chem. Lett.* **2013**, *4*, 127–131.
(40) Oh, S. H.; Black, R.; Pomerantseva, E.; Lee, J. H.; Nazar, L. F. Synthesis of a Metallic Mesoporous Pyrochlore as a Catalyst for Lithium–O_2 Batteries. *Nat. Chem.* **2012**, *4*, 1004–1010.
(41) Laoire, C. O.; Mukerjee, S.; Abraham, K. M.; Plichta, E. J.; Hendrickson, M. A. Elucidating the Mechanism of Oxygen Reduction for Lithium-Air Battery. *J. Phys. Chem. C* **2009**, *113*, 20127–20134.
(42) Laoire, C. O.; Mukerjee, S.; Abraham, K. M.; Plichta, E. J.; Hendrickson, M. A. Influence of Nonaqueous Solvents on the Electrochemistry of Oxygen in the Rechargeable Lithium-Air Battery. *J. Phys. Chem. C* **2010**, *114*, 9178–9186.
(43) Kang, S. Y.; Mo, Y. F.; Ong, S. P.; Ceder, G. A Facile Mechanism for Recharging Li_2O_2 in Li–O_2 Batteries. *Chem. Mater.* **2013**, *25*, 3328–3336.
(44) Lu, Y. C.; Shao-Horn, Y. Probing the Reaction Kinetics of the Charge Reactions of Nonaqueous Li–O_2 Batteries. *J. Phys. Chem. Lett.* **2013**, *4*, 93–99.
(45) Peng, Z. Q.; Freunberger, A. S.; Hardwick, L. J.; Chen, Y. H.; Giordani, V.; Bardé, F.; Novák, P.; Graham, D.; Tarascon, J. M.; Bruce, P. G. Oxygen Reactions in a Non-Aqueous Li^+ Electrolyte. *Angew. Chem., Int. Ed.* **2011**, *50*, 6351–6355.
(46) Hartmann, P.; Bender, C.; Sann, J.; Dürr, A. K.; Jansen, M.; Janek, J.; Adelhelm, P. A Rechargeable Room-Temperature Sodium Superoxide (NaO_2) Battery. *Phys. Chem. Chem. Phys.* **2013**, *15*, 11661–11672.
(47) Gerbig, O.; Merkle, R.; Maier, J. Electron and Ion Transport in Li_2O_2. *Adv. Mater.* **2013**, *25*, 3129–3133.
(48) Yilmaz, E.; Yogi, C.; Yamanaka, K.; Ohta, T.; Byon, H. R. Promoting Formation of Noncrystalline Li_2O_2 in the Li–O_2 Battery with RuO_2 Nanoparticles. *Nano Lett.* **2013**, *13*, 4679–4684.

(49) Bryantsev, V. S.; Blanco, M.; Faglioni, F. Stability of Lithium Superoxide LiO_2 in the Gas Phase: Computational Study of Dimerization and Disproportionation Reactions. *J. Phys. Chem. A* **2010**, *114*, 8165−8169.
(50) Hummelshøj, J. S.; Luntz, A. C.; Nørskov, J. K. Theoretical Evidence for Low Kinetic Overpotentials in Li-O_2 Electrochemistry. *J. Chem. Phys.* **2013**, *138*, 034703.